remote sensing

MDPI

Article

Persistent Scatterer Interferometry (PSI) Technique for the Identification and Monitoring of Critical Landslide Areas in a Regional and Mountainous Road Network

Constantinos Nefros [1,*], Stavroula Alatza [2], Constantinos Loupasakis [1] and Charalampos Kontoes [2]

[1] School of Mining and Metallurgical Engineering, National Technical University of Athens, Athens 15780, Greece
[2] Institute for Astronomy, Astrophysics, Space Applications and Remote Sensing, Center for Earth Observation Research and Satellite Remote Sensing BEYOND, National Observatory of Athens, Athens 15780, Greece
* Correspondence: kostasnefros@central.ntua.gr

Abstract: A reliable road network is a vital local asset, connecting communities and unlocking economic growth. Every year landslides cause serious damage and, in some cases, the full disruption of many road networks, which can last from a few days to even months. The identification and monitoring of landslides with conventional methods on an extended and complex road network can be a rather difficult process, as it requires a significant amount of time and resources. The road network of the Chania regional unit on the island of Crete in Greece is a typical example, as it connects, over long distances, many remote mountainous villages with other local communities, as well as with the main urban centers, which are mainly located across the shore. Persistent scatterer interferometry (PSI) is a remote-sensing technique that can provide a reliable and cost-effective solution, as it can be used to identify and monitor slow-moving and ongoing landslides over large and complex areas such as those of the mountainous road networks. This study applied PSI in the Chania regional unit, using the novel parallelized PSI (P-PSI) processing chain, developed by the Operational Unit Center for Earth Observation Research and Satellite Remote Sensing BEYOND of the Institute of Astronomy and Astrophysics, Space Applications and Remote Sensing of the National Observatory of Athens (BEYOND) for the rapid identification of the areas, most critical to landslide in a local road network. The application of P-PSI speeded up the total required processing time by a factor of five and led to the rapid identification and monitoring of 235 new slow-moving landslides. The identified landslides were correlated with a pre-existing landslide inventory and open access visual data to create a complete landslide inventory and a relative landslide inventory map, thus offering a valuable tool to local stakeholders.

Keywords: landslides; remote sensing; persistent scatterers; SAR; interferometry; GIS; spatial analysis; P-PSI; Sentinel-1; timeseries analysis.

Citation: Nefros, C.; Alatza, S.; Loupasakis, C.; Kontoes, C. Persistent Scatterer Interferometry (PSI) Technique for the Identification and Monitoring of Critical Landslide Areas in a Regional and Mountainous Road Network. *Remote Sens.* **2023**, *15*, 1550. https://doi.org/10.3390/rs15061550

Academic Editors: Joanne N. Halls, Chuanrong Zhang and Weidong Li

Received: 31 January 2023
Revised: 3 March 2023
Accepted: 10 March 2023
Published: 12 March 2023

1. Introduction

Throughout history, road networks have been essential for human societies, as they have been used for both passenger and freight transport [1]. Their good condition and safety are often considered paramount for socio-economic development [2,3]. Nowadays, despite the existence of many alternatives (such as railways and airports), road networks remain the main transportation infrastructure, especially in rural areas [3,4]. At the same time, the complexity of modern societies has led to a steady growth in transportation volume to cater to their everyday needs. According to McKinnon [5], if transportation by

trucks and lorries were halted, severe damage would occur to major sectors of the economy (such as the food supply, hospital–medicine supplies, rubbish management) in only four days, pushing parts of society into complete chaos.

In Greece, most of the regional road networks consist of one or two lanes in each direction [6], rendering the whole network extremely vulnerable to landslides. Consequently, in roads connecting villages in mountainous areas, even a single event can cause serious damage to, or even result in the full disruption of, the road network. For example, during medicane (Mediterranean tropical-like cyclone) Ianos, which affected several regions in Greece from 18 to 20 September 2020, devastating landslides were activated that blocked several local, narrow, mountainous roads, leading to several villages being cut off [7]. Moreover, the mountainous landscape and the inexistence of any alternative routes significantly delayed emergency response and restoration efforts by the authorities [7]. These severe impacts highlight the value of developing a process for the rapid and effective identification and monitoring of the landslides in a regional and mountainous road network. This, however, comes with many difficulties, such as the inexistence of a complete local landslide inventory and the usually large extent of the road network.

According to [8,9], landslides tend to be repeated under the same or similar conditions in areas where they have occurred in the past. Hence, a complete landslide inventory, which includes as many of the landslides that have occurred in a study area as possible, could be a helpful decision-making guide, as it provides direct indications for potential future landslides. Moreover, it can help researchers identify more effectively which, and to what extent, of the local factors (e.g., slope, aspect, precipitation, proximity to rivers/faults) are correlated with the local landslide mechanism [10]. However, in many countries, a national landslide inventory does not exist [11]. In addition, many landslides, and especially the slow-moving ones, are not recorded at all. This is because small rocks or mudflows, which can be the result of such events, are rapidly removed from the road pavement by the authorities in their attempt to restore road traffic/circulation as quickly as possible [7]. However, besides its significant contribution to the formation of a complete landslide inventory, mapping of slow-moving landslides can also provide evidence of micro-ground movements with a precision of millimeters or centimeters, which can be a critical indication of an evolving landslide [12].

Moreover, mapping of slow-moving landslides over an extended area, such a regional road network, requires significant resources and time. Conventional methods, such as the installation of inclinometers and piezometers, are not a cost-effective solution, mostly due to the large extent of a regional road network [11].

Persistent scatterers (PS) [13] and small baseline subset (SBAS) [13], are interferometry synthetic aperture radar (InSAR) methods [14] that have been progressively used over the last years for the systematic mapping and recording of slow-moving landslides [12,15]. While both methods have been proved to be rather effective, PS appears to be slightly more accurate compared to SBAS [16], and was therefore selected for this study. An extensive analysis and comparison of these InSAR techniques is provided by [13,16].

Since PS is basically a remote-sensing technique, which uses open access SAR images as well, it has the advantage of not intervening with the examined area [17], which makes it a low-cost and, at the same time, a rather effective method. In addition, it can be applied over an extended area [17], such as a regional road network, and can cover a long period of time [18]. However, the processing of such a large volume of data is a time-consuming procedure, which can render the method invalid for the rapid identification of landslides or the regular update-monitoring of an existing database. Therefore, the use of the parallel PSI (P-PSI) processing chain [15], developed by the Operational Unit Center for Earth Observation Research and Satellite Remote Sensing BEYOND of the Institute of Astronomy and Astrophysics, Space Applications and Remote Sensing of the National Observatory of Athens (BEYOND), significantly contributed to minimizing the processing time of Sentinel-1 data. The efficiency of P-PSI compared to a typical InSAR time-series analysis lies in the parallelization of time-consuming processing steps. Taking advantage of parallel

resources, an overall speed-up of up to five times is achieved compared to a typical PSI [13]. Algorithmic interventions are performed to existing open-source PSI software, creating a parallelized, fully-automated PSI processing chain tailored to big data SAR processing. Recent studies exploit the potentiality of applying the PS method in combination with efficient and automated processes for the detection of structural deformations, either on individual elements of a road network, such as bridges [19], or on large parts of road networks [20]. These studies automate the whole procedure and provide critical insights about the potentiality of PS, and have therefore been applied to different areas in Italy (the highway and motorway networks of Rome and Bari), as well as in the USA (Los Angeles highway and freeway network). While both [19,20] methods are very effective and novel, they are based on Geographical Information System (GIS) algorithms, which are applied after the production of the PS, which, as was mentioned before, can be a rather time-consuming procedure. Thus, while a significant part of the whole process is accelerated by using these methods, a critical part of the process is left out, i.e., the processing of the large volume of satellite data that is needed to produce the PS.

To overcome this limitation, the parallelized-persistent scatterer interferometry (P-PSI) chain, which was developed by the BEYOND center, can be applied, as it can speed up the PS production by a factor of five [21].

The main aim of this study is to present how P-PSI along with GIS techniques can be used to identify and monitor slow-moving landslides across an extended and complex geomorphological road network, thereby providing an initial and rapid indication of potentially ongoing landslides. These findings, along with an existing landslide inventory, can then be used to create a complete landslide inventory map, providing an overall estimation of the condition of the regional road network. The acquired information can be a valuable guide for stakeholders interested in putting in place prevention measures. At the same time, based on its rapid and low-cost applicability, the presented method can be further used as a tool for the periodical examination of the efficiency of these measures and for the re-estimation of the condition of the road network.

In this direction, the Chania regional unit on Crete Island, Greece, is selected as a case study, due to its rather extended and complex geomorphological road network. It is significant to note that this study mostly focuses on potential landslides occurring on the cuttings of the road network, rather on the potential subsidence of its embankments.

2. Study Area

The Chania regional unit is one of the four administrative regions of Crete Island, Greece, with an extent of over 2.000 km^2. It borders at the north with the Cretan Sea, at the west with the Ionian Sea and at the south with the Libyan Sea. As illustrated in Figure 1, it has a rather complex landscape as it combines an extended coastline with hilly and mountainous areas.

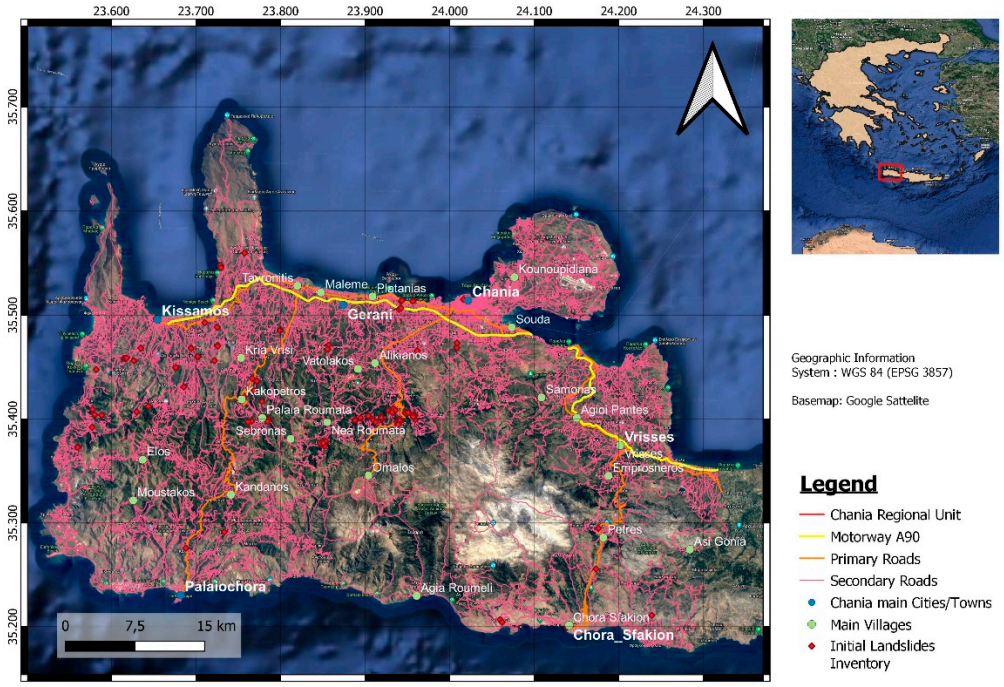

Figure 1. Chania road network.

Most of the biggest cities are located on or near the shore, while most of the villages are located inland, where hills and mountains mostly dominate. As a result, the road network that has been developed over the years follows the relative local landscape and connects over long distances mountains and lowland areas.

The diverse and extended terrain has progressively led to the development of a rather dense and complicated road network. In the north, the road network consists of a large part of motorway A90, which mostly stretches along the shoreline and is the longest and most important road in Crete. A90 mainly consists of one lane (and in some regions two lanes) in each direction separated sometimes by a median barrier, plus an emergency lane. Furthermore, three primary roads branch out from motorway A90, connecting the plains of the north with the mountainous regions of the south. These primary roads have a north–south direction and usually consist of one lane in each direction, plus an emergency line, and lack a median barrier. A great part of the Chania south is characterized by a relatively intense relief, which in some cases exceeds 2.000 m. Several smaller secondary roads connect the various communities of the area. They usually consist of only one lane in both directions, while an emergency lane either does not exist or is very narrow and therefore inadequate even for stranded vehicles to use in case of an emergency. Due to their small size, and the usual lack of precautionary measures, these parts of the road network are expected to be the most vulnerable to landslides.

There are ten main geological formations which dominate the study site, with Phyllites–Quartzites in the west and Plattenkalk Limestones (mainly consisting of schists, dolomites, limestones, evaporites, and quartzites) in the east being the major ones. Trypalion carbonate formations are found between these two formations, from the south up until the northeast at Souda's Bay, as well as in the easternmost peninsula of the regional unit. Tripolis Carbonate formations are observed at the other two peninsulas of the region, which are located at the northwest of the examined area. At the same time, Neogene sediments are mostly located in the northwest and northeast of the regional unit, while small concentrations are found at its southwest shores. Quaternary Deposits Alluvium covers many different sections, which are mostly located in the west of the examined area. Finally, Flysch Tripolis, Ophiolite complex, and Pindos Carbonates cover the remaining

smaller and dispersed regions of the examined area. Due to the extensive geological fragmentation, landslide activity on the road network is expected to be frequent. A more detailed description of the geology of Chania regional unit, along with its geological map, can be found in [22].

3. Data and Methods

3.1. Data

For this study, satellite, landslide, and visual data were used. The following sub-sections outline them in greater detail.

3.1.1. Sentinel Data

Sentinel images are high-resolution satellite images provided freely by the European Satellite Agency (ESA) as part of the Copernicus program [23]. Sentinel-1 are radar satellite images received at C-Band (5.405 GHz) that can provide all-weather, day-and-night information [24]. During this study, Sentinel-1 interferometric wide swath (IW) single look complexes (SLC) were downloaded for the period spanning 2016 to 2020 from the Alaska satellite facility (ASF) hub. Sentinel images were selected due to their short repeat cycle of the satellite mission, which, for the same geometry, is down to 6 days (or 12 days when using only one satellite) [25]. Thus, they provide a quite sufficient temporal coverage of the area of interest. Information on the data used is summarized in Table 1.

Table 1. Characteristics of the Sentinal-1 images processed and of the created products.

Orbit	Path	Frame	Examined Period		Number of Interferograms	Number of PS
			From	To		
Ascending	102	113	19/9/2016	27/12/2020	98	291.234
Descending	109	473	8/10/2016	22/12/2020	90	382.017

The extent of the examined area, spatially covered by almost an entire Sentinel frame, and of the examined period, which spans close to 4 consecutive years, resulted in the creation of large stacks of radar satellite images of more than 2 Terabytes.

3.1.2. Landslide Inventory Data

An initial landslide inventory was created by using landslide data derived from the Hellenic Survey of Geology and Mineral Exploration (HSGME). The inventory was enriched by landslide data from literature [22,26] and concerns only landslides that occurred on the slopes affecting the road network. The initial landslide inventory that was created consists of 130 landslides and is illustrated in Figure 1.

3.1.3. Visual Data

The visual data used were obtained either with in situ investigations or open access sources such as historical street view images (such as google, mapillary and kartaview street view) and google satellite images. These data were obtained only for the specific critical areas of the initial landslide inventory and for the slow-moving landslides determined with P-PSI. Otherwise, the required processing time for the examination of such an extended road network would lead to serious delays and would render the whole method inefficient. Moreover, these data are freely available and regularly enriched with more up-to-date images. Thus, they can contribute to the regular, direct, and rapid update of the following method.

3.2. Methodology

In general, the methodology followed consists of three steps. Initially, the P-PSI chain is implemented to determine the line-of-site (LOS) displacements of the PSs for the ascending and the descending satellite passes. Next, the LOS PSI displacements are analyzed along with visual data, to evaluate the slow-moving landslides of the study area. Finally, the slow-moving landslides are used to identify potential ongoing landslides. The slow-moving landslides and the landslides provided by the initial landslide inventory are then merged in a new file, which provides an integrated and complete landslide inventory of the examined road network. It is significant to note that each of these landslides retains their origin (slow-moving landslide or initial inventory) as an attribute record. Using the produced complete landslide inventory, a relative landslide inventory map is created, which shows the region's most critical to landslide in the examined area. Figure 2 provides an overview of the methodology followed.

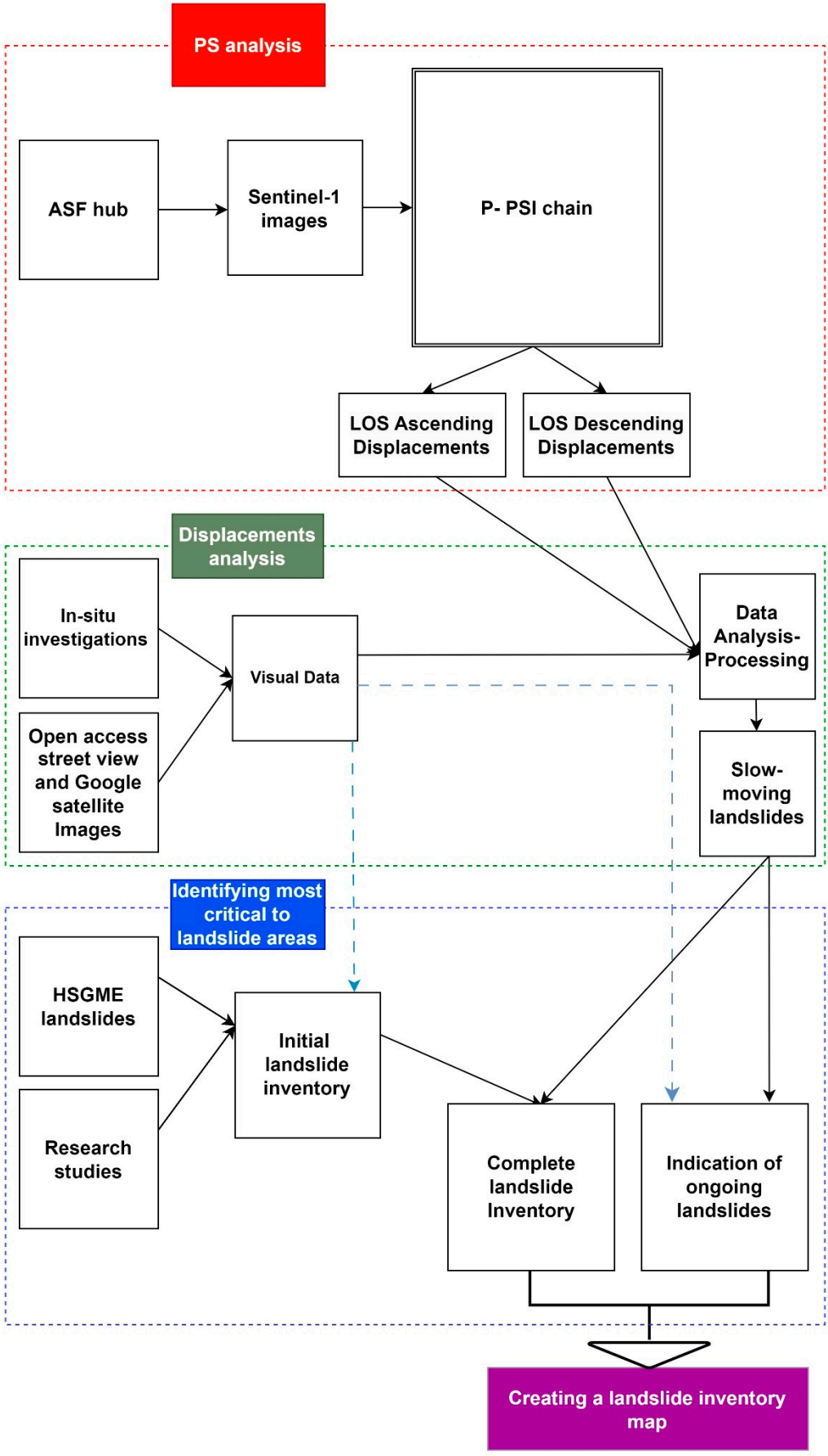
PS analysis
ASF hub
Sentinel-1 images
P- PSI chain
LOS Ascending Displacements
LOS Descending Displacements
Displacements analysis
In-situ investigations
Open access street view and Google satellite Images
Visual Data
Data Analysis-Processing
Slow-moving landslides
Identifying most critical to landslide areas
HSGME landslides
Research studies
Initial landslide inventory
Complete landslide Inventory
Indication of ongoing landslides
Creating a landslide inventory map

Figure 2. Flowchart of the methodology followed.

3.2.1. Persistent Scatterers (PS) Analysis

InSAR techniques have been widely used over the last years for detecting ground deformations, such as earthquakes [27] and landslides [21]. Persistent scatterer interferometry (PSI) is an InSAR technique used for the identification of landslide events [28], as it has been proven to be rather effective, especially in difficult-to-access areas, where conventional methods usually fail to provide reliable results [12]. The PSI technique is based on the characteristics of some objects, such as outcropping rocks and buildings, to backscatter the radar signal differently due to their shape or their multispectral reflectance. Based on the difference between the phase of the emitted and the received signal of these objects, so-called persistent scatterers (PS), useful information can be extracted about the deformation of the surface.

However, PS analysis can be a rather time-consuming technique when applied in a broad area [29], such as the road network examined in this study. To address this problem, the parallelized persistent scatterer interferometry (P-PSI) processing chain was applied. P-PSI is a novel InSAR technique that was created by the BEYOND center. P-PSI accelerates the whole process by using distributed computing techniques and prioritizing the time-bottleneck and the most demanding processing tasks [21], such as the parallelized InSAR Scientific Computing Environment (ISCE), which is used for the stacks' creation, and the parallelized Stanford method for persistent scatterers (StaMPS), which is used for the multi-temporal SAR interferometry [30]. The open-source Toolbox for Reducing Atmospheric InSAR Noise (TRAIN) was also used to remove the effects of the atmosphere in the created interferograms. As a result, the PS line-of-sight (LOS) displacements for the ascending and descending orbits were determined (Figure 2).

3.2.2. Displacements Analysis

As already explained, PSI can be used to detect extremely slow-moving ground movements with millimeter precision [12]. However, over an extended area, such as the one examined, the identification of slow-moving landslides based on the examination of each PS can be a rather difficult and cumbersome process due to the large number of generated PSs. In our case, as shown in Table 1, the PSs resulting from the PSI analysis were over 650.000.

Thus, it is critical to reduce the PS number. This can be achieved through GIS techniques and PS clustering, as explained in the following paragraphs. Subsequently, visual data derived from in situ investigations and open access data can be used in a GIS environment, along with the areas' special features, to identify slow-moving landslides along with their characteristics, such as their orientation and the limits of their spatial extension.

3.2.3. Identifying Areas Most Critical to Landslide

According to Wang [31], before a landslide event there is always some micro-displacement. Thus, the examination of previously identified slow movements over a region, in conjunction with the prevailing local hydrological and geomorphological characteristics of the area, as well as pertinent visual data, can provide critical indications of potential ongoing landslide events. Due to the short repeat cycle of the Sentinel satellite mission, the described process can be regularly updated, providing further up-to-date information concerning landslides' activation, which can be from 1 to 3 days old. Thus, the followed method, due to its direct and rapid applicability, even in such an extended area, can be part of a low-cost early warning system used to monitor landslides' activity. To this end, recent visual data can be also used to validate the effectiveness of this method (Figure 2).

Furthermore, as illustrated in Figure 2, the spatial recording of the slow-moving landslides can also contribute to the formation of a complete landslide inventory. In some

cases, slow-moving landslides are not recorded, and the created inventories are incomplete. However, a complete landslide inventory is very significant as it can aid researchers to better understand the function of the local landslide mechanism and to identify the hydrological and geomorphological causal factors that can lead to its activation. Moreover, they can also be used to update the elements of an existing landslide inventory, such as the geometry and extent of previously recorded landslides, their orientation, or their status of activity. Therefore, following the aforementioned procedure, a complete landslide inventory can be formed.

3.2.4. Landslide Inventory Map (LIM)

The landslide inventory maps (LIMs) show the locations where landslides have occurred in the recent or distant past, providing simple and direct indications about possible future landslides [29]. Their biggest advantage is that they can be easily, directly, and rapidly used to acquire the necessary information, without requiring any prior experience or knowledge.

Thus, the creation of a LIM, which can be easily and effectively updated in a short period and at a low cost, over an extended area, such as the examined road network of the Chania regional unit, can be a valuable tool for local stakeholders.

4. Results and Discussion

4.1. Implementing the P-PSI Chain

As shown in Figure 2, after downloading the necessary Sentinel-1 images from ASF hub, the P-PSI chain was used to evaluate the line-of-sight (LOS) displacements for both ascending and descending orbits.

A common reference area that is expected to be relatively stable must be selected for the produced stacks [15]. Moreover, this area must be away from agricultural fields, to avoid possible seasonal deformations due to pumping activities [32]. Thus, an area of low relief at the outskirts of Chania City was selected as the reference area.

Subsequently, an image was selected as the main image to obtain the minimum temporal and perpendicular baselines. This image was that of 21 October 2018 for the ascending orbit and of 13 April 2019 for the descending orbit. These images were characterized as the "primary" image for each orbit, while the rest were characterized as "secondary".

Afterwards, the relative standard deviation was evaluated to determine the outliers from the mean PS velocities and to estimate the noise on the LOS deformation velocities [12]. These outliers were discarded as they were affected by the temporal decorrelation and the atmospheric noise created by the local topography, in order for the final standard deviation values to be under 2. Figure 3 illustrates the LOS displacements that were created for both the ascending and descending orbits.

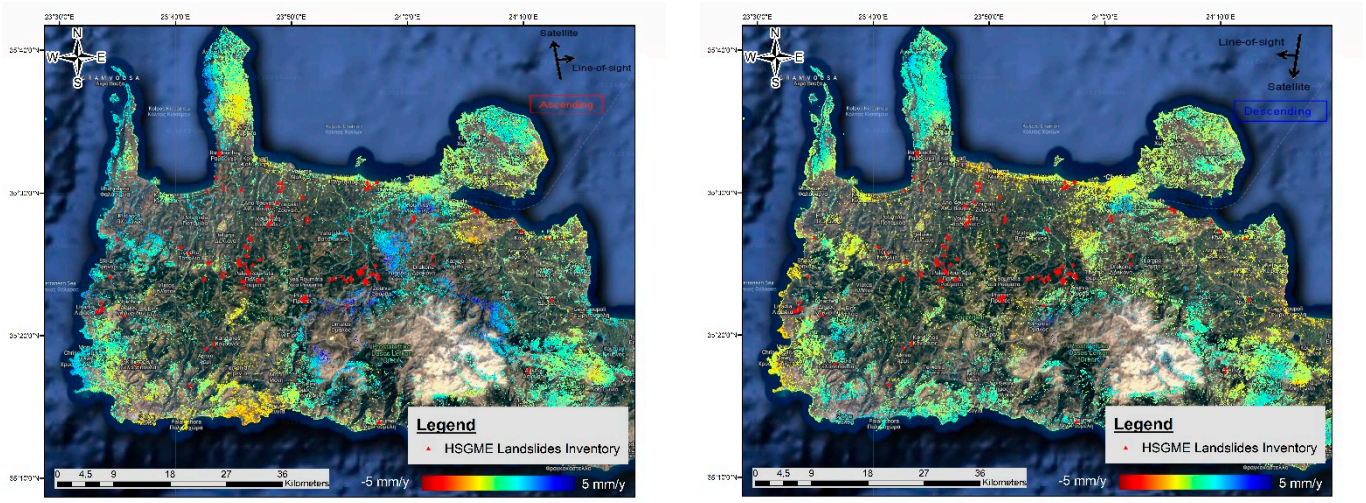

(**a**) (**b**)

Figure 3. LOS displacements for the ascending (**a**) and descending (**b**) satellite pass, along with the initial landslide inventory provided by the HSGME.

It should be noted that the LOS displacement velocities of the examined area are up to 6 mm/year, which is a regular value compared to the results of other studies in regions with similar geomorphological characteristics [32]. In some cases, relatively high values of negative-sign velocities were recorded, mainly at the peak of the Lefka Ori mountain. These results are due to the climatic conditions that usually dominate in that area, as suggested by previous studies [33].

However, the method did not provide enough PSs over densely vegetated regions, which was expected due to the inherent difficulty of InSAR methods to identify PSs over such areas.

4.2. Identifying Landslides

From the PSI analysis, the LOS displacement deformations were evaluated, creating a large number of PSs (as shown in Table 1). To overcome this problem and reduce the number of PSs, GIS techniques were applied to identify which of these PSs are associated with the road network.

Thus, as a first step, it was determined for both the ascending and descending orbit which of the PS LOS displacement deformations were close to the road network (i.e., closer than 50 m, 30 m, and 20 m at each side of the motorway's, the primary roads', and the secondary roads' central line markings, respectively), and the rest of them were discarded.

To further reduce the number of examined cases, the PSs should be clustered into groups or classes [25], providing a recent example of PSI clustering over a large area. Thus, the PSs were clustered according to their LOS velocity [17]. It is significant to note that the reduction in the PS number was also automated by applying the Model Builder tool of the open access QGIS software to combine a series of individual GIS tools such as:

- the buffer tool to create linear surfaces in 50 m, 30 m, and 20 m at each side of the motorway's, the primary roads', and the secondary roads' central line markings, respectively,
- select by location to include only the PSs that intersect with these surfaces, and
- select by expression to exclude the PS movements with a velocity smaller than the threshold of −2 mm per year.

Due to the significantly reduced number of areas most critical to landslide, and based also on visual data (e.g., Google Earth historical satellite images), as well as the local hydrological and geomorphological characteristics of the examined area, it was feasible to

rapidly identify slow-moving landslides. Figure 4 illustrates the use of visual data to identify slow-moving landslides in the entrance to Askifou village.

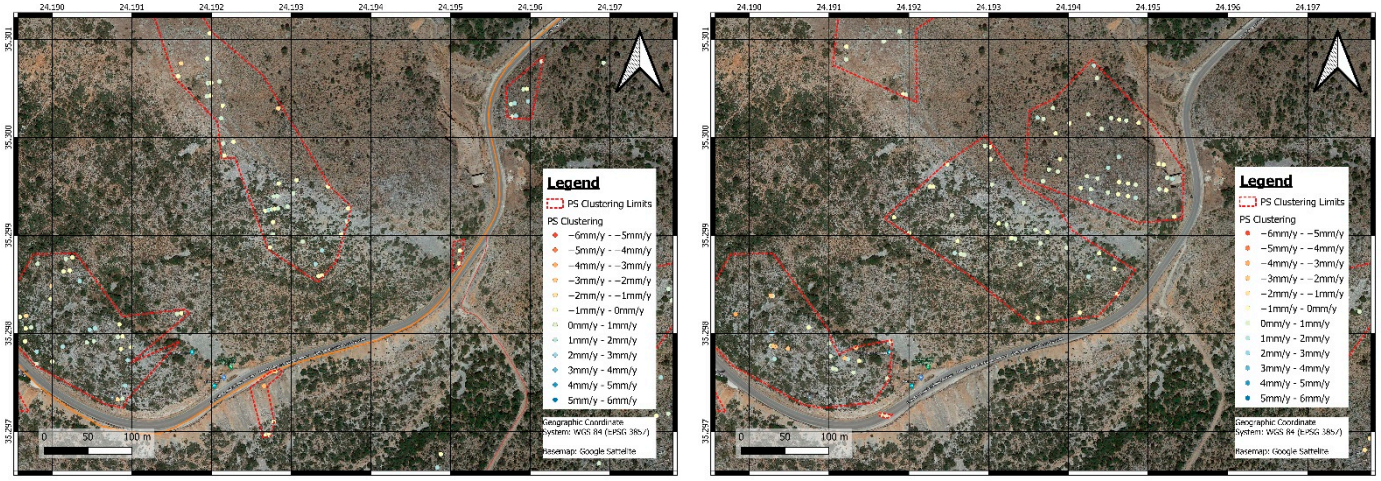

(**a**) (**b**)

Figure 4. Identification of a slow-moving landslide on the road outside Askifou village [34] for the (**a**) ascending satellite pass and for the (**b**) descending satellite pass.

It is important to note that, as was expected, the majority of the identified slow-moving landslides were not included in the pre-existing landslide inventory. This finding, which is consistent with the findings of other studies [12], highlights the significance of recording slow-moving landslides in order to acquire a complete landslide inventory.

Furthermore, as was previously mentioned, a slow-moving landslide can be the initial evolvement of an ongoing landslide. Indeed, as shown in Figure 5, the slope over the road network in the entrance of the Macheri village was between the areas where micro-movements were identified and where a landslide also occurred in December of 2021 (outside of the examined time period) [35].

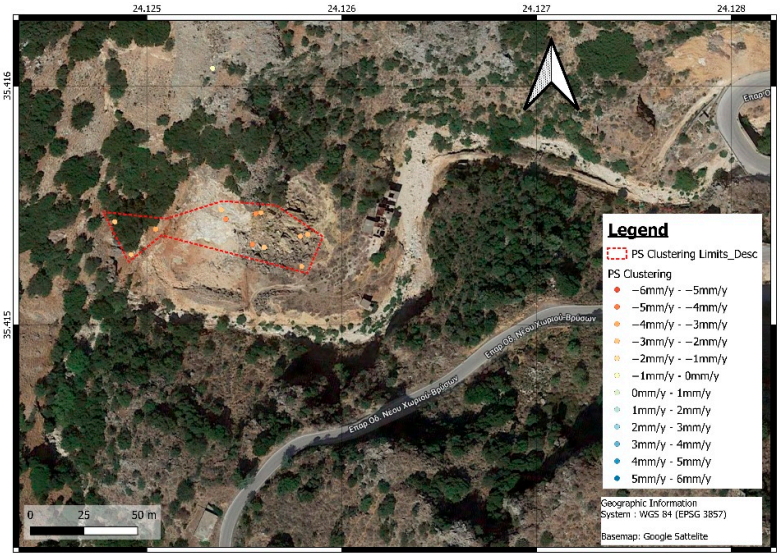

Figure 5. Identification of potential ongoing landslide events in the entrance of the Macheri village [36].

Moreover, as shown in Figure 2, visual data were used to enrich the characteristics of the initial landslide inventory. Thus, as shown in Figure 6, visual data derived from

google street view were used to identify a past landslide event that was reactivated on the local road that connects Tavronitis village with Paleochora town.

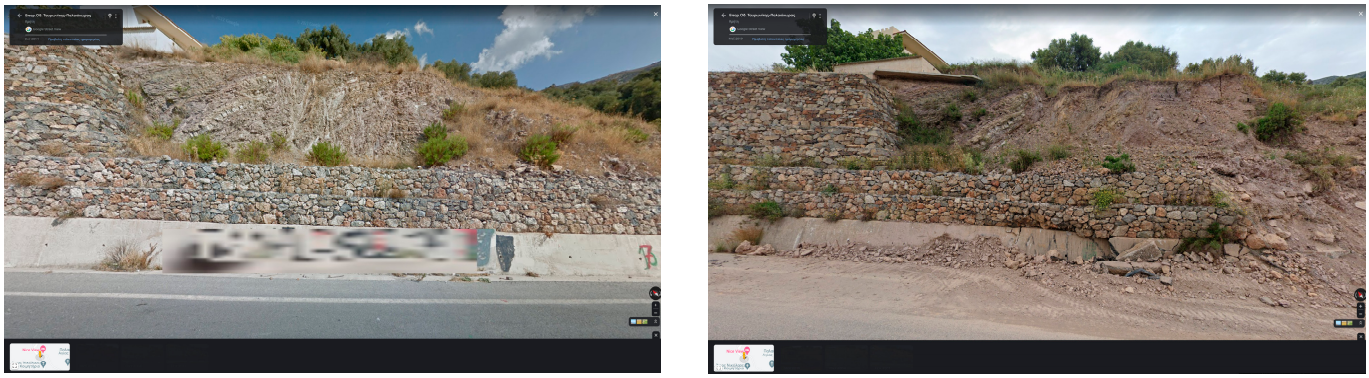

(**a**) (**b**)

Figure 6. Enriching the landslide inventory about the activity status of an existing landslide in the road connecting Tavronitis village with Palaiochora city using Google Street view: (**a**) Image obtained in 2014 [37]; (**b**) Image obtained in 2019 [38].

Relatedly, as shown in Figure 7, visual data derived from open access sources can also be used to monitor the evolution of an ongoing landslide and the effectiveness of the applied protective measures.

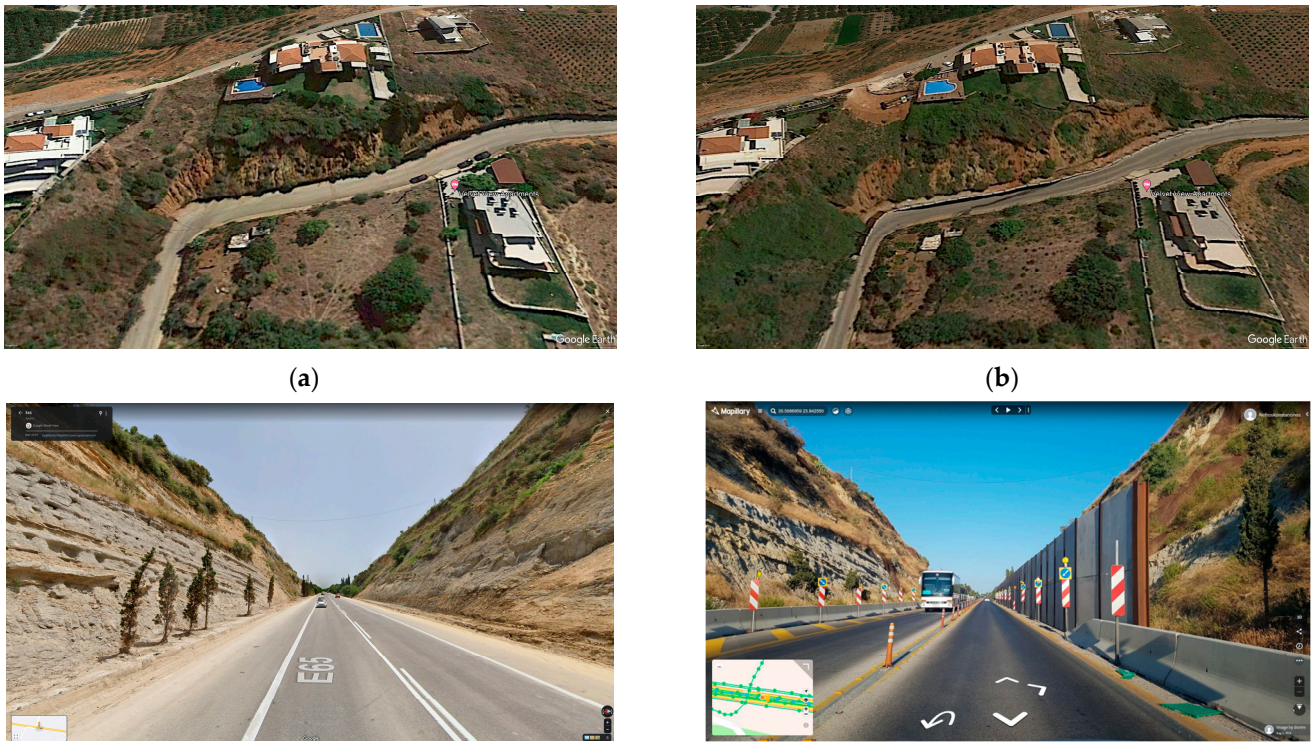

(**a**) (**b**)

(**c**) (**d**)

Figure 7. Monitoring of potential ongoing landslide events using open access data of: (**a**) Google Earth Satellite view at Stalos village Jun 2013 [39]; (b) Google Earth Satellite view at Stalos village March 2022 [40]; (**c**) Google Street view at motorway A90 outside Stalos village May 2019 [41]; (**d**) Mapillary Street view at motorway A90 outside Stalos village [42].

Consequently, as a result of the acquired information, further preventive actions can be adopted by the authorities to stabilize the slope.

4.3. Creating the Landslide Inventory Map

The complete formed landslide inventory, consisting of 365 landslides, was used to create the landslide inventory map (LIM) of the examined road network of the Chania regional unit, which is provided in Figure 8.

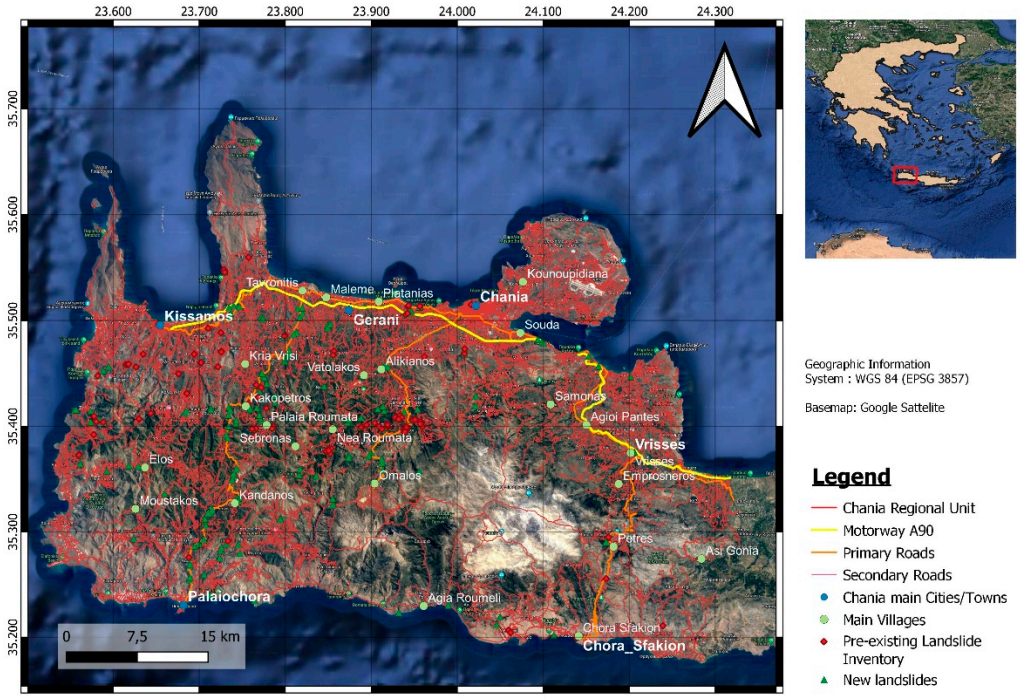

Figure 8. Landslide inventory map of the road network of Chania regional unit.

The inventory includes 130 landslides of the initial landslide inventory and 235 landslides identified using the P-PSI process. The produced LIM allows the direct, simple, and rapid identification of the regions, most critical to landslides. It can therefore be used by the authorities for the identification of the areas, most prone to landslide that require the implementation of support measures to stabilize the slope.

Based on the created LIM, the following road sections along the motorway A90 were identified as rather prone to landslide events. The road sections where stakeholders should focus their preventive measures for a potential landslide are:

- Kissamos to Tavronitis (near Nopigia village),
- Platanias to Chania (near Stalos and Kato Galatas villages), and
- Souda to Agioi Pantes (near Platani, Megala Chorafia, Kalami, and Kalives villages).

The large number of identified landslides, even at the motorway A90, the largest on Crete Island, also highlights the value of a complete and accurate geotechnical study during road construction.

Due to the LIM's ability to be easily updated with recent satellite data, it can also act as an early warning system [20], providing authorities with the necessary time to either:

- apply preventive measures for stabilizing the slope on that particular section of the road network, or, if this is not feasible.
- prevent citizens from using it and identify safer alternative routes in the existing road network.

Moreover, the LIM can be used to identify safer areas less prone to landslide. It can therefore be effectively used by authorities during land use/land planning processes, such as, for example, when seeking appropriate and safe areas for constructing new motorways. Supplementary Material Figures S1–S4 and Supplementary Material Tables S1–S4

provide the statistical comparison of new landslides with the initial landslide inventory, according to the outcropping geology, the slope angle, the slope aspect, and the type of relief.

The present study identified the areas, most prone to landslide of a rather complex road network by applying the P-PSI chain along with GIS techniques, an initial landslide inventory, and visual data. Yet, the combination of the proposed GIS techniques with those proposed by other studies [19,20] is proposed as an area for future work, which can help examine if further acceleration of the whole process is being achieved.

5. Conclusions

As shown in this study, the P-PSI chain performed rather well in identifying slow-moving landslides. It provided adequate and accurate information that was used to identify more than 235 new slow-moving landslides. Moreover, it provided evidence for ongoing landslides, while at the same time it was used to enrich the existing initial landslide inventory.

The combination of the existing landslide inventory with the identified slow-moving landslides is significant, as it can help researchers understand which factors, and to what extent, are responsible for a landslide event. Moreover, the potentiality of PSI's applicability for rapidly, and at low cost, identifying and monitoring landslide events over a road network was also presented. Furthermore, the augmented value of the open access visual data for the identification and the temporal monitoring of the landslides was also highlighted by this study.

The applied method, because of its rapid and low-cost applicability, can be used for the systematic enrichment and updating of landslide inventories, even on extended and complex road networks, such as the one in the Chania regional unit. Thus, it can be a valuable tool for local stakeholders, as it can provide complete and easy-to-use landslide inventory maps, while at the same time it can also act as part of an early warning system for monitoring ongoing landslides.

Supplementary Materials: The following supporting information can be downloaded at: https://www.mdpi.com/article/10.3390/rs15061550/s1, Supplementary Material Figure S1: statistical comparison of new landslides with the initial landslide inventory, according to the outcropping geology ; Figure S2: statistical comparison of new landslides with the initial landslide inventory, according to the slope angle; Figure S3: statistical comparison of new landslides with the initial landslide inventory, according to the slope aspect; Figure S4: statistical comparison of new landslides with the initial landslide inventory, according to the type of relief; Supplementary Material Table S1: statistical comparison of new landslides with the initial landslide inventory, according to the outcropping geology ; Table S2: statistical comparison of new landslides with the initial landslide inventory, according to the slope angle; Table S3: statistical comparison of new landslides with the initial landslide inventory, according to the slope aspect; Table S4: statistical comparison of new landslides with the initial landslide inventory, according to the type of relief.

Author Contributions: Conceptualization: C.N. and C.L.; Data curation: C.N. and S.A.; Formal analysis: C.N. and S.A.; Investigation: C.N. and S.A.; Methodology: C.N., C.L., and C.K.; Project administration: C.L. and C.K.; Resources: C.K.; Software: C.N., S.A., and C.K.; Supervision: C.L.; Validation: C.N. and C.L.; Visualization: C.N. and C.L.; Writing—original draft: C.N.; Writing—review and editing: S.A., C.L., and C.K. All authors have read and agreed to the published version of the manuscript.

Funding: This research received no external funding.

Data Availability Statement: The data used to support the findings of this study are available from the corresponding author upon reasonable request.

Acknowledgments: Sentinel-1 images were processed with the P-PSI processing chain in the Operational Unit Center for Earth Observation Research and Satellite Remote Sensing BEYOND of the Institute of Astronomy and Astrophysics, Space Applications and Remote Sensing of the National

Observatory of Athens (BEYOND). The pre-existing landslide inventory was provided by the Hellenic Survey of Geology and Mineral Exploration (HSGME).

Conflicts of Interest: The authors declare no conflicts of interest.

References

1. Engström, R. The Roads' Role in the Freight Transport System. *Transp. Res. Procedia* **2016**, *14*, 1443–1452. https://doi.org/10.1016/j.trpro.2016.05.217.
2. Nikolaeva, R.V. Road Safety as a Factor in the Socio-Economic Development of the Country. *IOP Conf. Ser. Mater. Sci. Eng.* **2020**, *786*, 012070. https://doi.org/10.1088/1757-899X/786/1/012070.
3. Ivanová, E.; Masárová, J. Importance of road infrastructure in the economic development and competitiveness. *Econ. Manag.* **2013**, *18*, 263–274. https://doi.org/10.5755/j01.em.18.2.4253.
4. Kongolo, M. Perceived Role of Rural Roads in Supporting and Enhancing Rural and Agricultural Development in Mwanza Region, Tanzania. *Issues Soc. Sci.* **2020**, *8*, 31. https://doi.org/10.5296/iss.v8i1.17067.
5. McKinnon, A. Life without trucks: The impact of a temporary disruption of road freight transport on a national economy. *J. Bus. Logist.* **2006**, *27*, 227–250. https://doi.org/10.1002/j.2158-1592.2006.tb00224.x.
6. Psarianos, B.; Stamatiadis, N. Speed Management in Rural Roads in Greece. *J. Civ. Eng. Archit.* **2012**, *6*, 1083. https://doi.org/10.17265/1934-7359/2012.09.001.
7. Valkaniotis, S.; Papathanassiou, G.; Marinos, V.; Saroglou, C.; Zekkos, D.; Kallimogiannis, V.; Karantanellis, E.; Farmakis, I.; Zalachoris, G.; Manousakis, J.; et al. Landslides Triggered by Medicane Ianos in Greece, September 2020: Rapid Satellite Mapping and Field Survey. *Appl. Sci.* **2022**, *12*, 12443. https://doi.org/10.3390/app122312443.
8. Malamud, B.D.; Turcotte, D.L.; Guzzetti, F.; Reichenbach, P. Landslide Inventories and Their Statistical Properties. *Earth Surf. Process Landf.* **2004**, *29*, 687–711. https://doi.org/10.1002/esp.1064.
9. Samia, J.; Temme, A.; Bregt, A.K.; Wallinga, J.; Stuiver, J.; Guzzetti, F.; Ardizzone, F.; Rossi, M. Implementing Landslide Path Dependency in Landslide Susceptibility Modelling. *Landslides* **2018**, *15*, 2129–2144. https://doi.org/10.1007/s10346-018-1024-y.
10. Nefros, C.; Loupasakis, C. Introducing a Geospatial Database and GIS Techniques as a Decision-Making Tool for Multicriteria Decision Analysis Methods in Landslides Susceptibility Assessment. *Bull. Geol. Soc. Greece* **2022**, *59*, 68–103. https://doi.org/10.12681/bgsg.29038.
11. van Westen, C.J.; van Asch, T.W.J.; Soeters, R. Landslide Hazard and Risk Zonation—Why Is It Still so Difficult? *Bull. Eng. Geol. Environ.* **2006**, *65*, 167–184. https://doi.org/10.1007/s10064-005-0023-0.
12. Aslan, G.; Foumelis, M.; Raucoules, D.; de Michele, M.; Bernardie, S.; Cakir, Z. Landslide Mapping and Monitoring Using Persistent Scatterer Interferometry (PSI) Technique in the French Alps. *Remote Sens.* **2020**, *12*, 1305. https://doi.org/10.3390/rs12081305.
13. Crosetto, M.; Monserrat, O.; Cuevas-González, M.; Devanthéry, N.; Crippa, B. Persistent Scatterer Interferometry: A Review. *ISPRS J. Photogramm. Remote Sens.* **2016**, *115*, 78–89. https://doi.org/10.1016/j.isprsjprs.2015.10.011.
14. Nikos, S.; Ioannis, P.; Constantinos, L.; Paraskevas, T.; Anastasia, K.; Charalambos (Haris), K. Land Subsidence Rebound Detected via Multi-Temporal InSAR and Ground Truth Data in Kalochori and Sindos Regions, Northern Greece. *Eng. Geol.* **2016**, *209*, 175–186. https://doi.org/10.1016/j.enggeo.2016.05.017.
15. Papoutsis, I.; Kontoes, C.; Paradissis, D. Multi-Stack Persistent Scatterer Interferometry Analysis in Wider Athens, Greece. *Remote Sens.* **2017**, *9*, 276. https://doi.org/10.3390/rs9030276.
16. Pasquali, P.; Cantone, A.; Riccardi, P.; Defilippi, M.; Ogushi, F.; Gagliano, S.; Tamura, M. Mapping of Ground Deformations with Interferometric Stacking Techniques. In *Land Applications of Radar Remote Sensing*; InTech: 2014; London; UK.
17. D'Aranno, P.J.V.; di Benedetto, A.; Fiani, M.; Marsella, M.; Moriero, I.; Palenzuela Baena, J.A. An Application of Persistent Scatterer Interferometry (PSI) Technique for Infrastructure Monitoring. *Remote Sens.* **2021**, *13*, 1052. https://doi.org/10.3390/rs13061052.
18. Ferretti, A.; Prati, C.; Rocca, F. Permanent Scatterers in SAR Interferometry. *IEEE Trans. Geosci. Remote Sens.* **2001**, *39*, 8–20. https://doi.org/10.1109/36.898661.
19. Nettis, A.; Massimi, V.; Nutricato, R.; Nitti, D.O.; Samarelli, S.; Uva, G. Satellite-Based Interferometry for Monitoring Structural Deformations of Bridge Portfolios. *Autom. Constr.* **2023**, *147*, 104707. https://doi.org/10.1016/j.autcon.2022.104707.
20. Macchiarulo, V.; Milillo, P.; Blenkinsopp, C.; Giardina, G. Monitoring Deformations of Infrastructure Networks: A Fully Automated GIS Integration and Analysis of InSAR Time-Series. *Struct. Health Monit.* **2022**, *21*, 1849–1878. https://doi.org/10.1177/14759217211045912.
21. Papoutsis, I.; Kontoes, C.; Alatza, S.; Apostolakis, A.; Loupasakis, C. InSAR Greece with Parallelized Persistent Scatterer Interferometry: A National Ground Motion Service for Big Copernicus Sentinel-1 Data. *Remote Sens.* **2020**, *12*, 3207. https://doi.org/10.3390/rs12193207.
22. Nefros, C.; Tsagkas, D.S.; Kitsara, G.; Loupasakis, C.; Giannakopoulos, C. Landslide Susceptibility Mapping under the Climate Change Impact in the Chania Regional Unit, West Crete, Greece. *Land* **2023**, *12*, 154. https://doi.org/10.3390/land12010154.
23. Showstack, R. Sentinel Satellites Initiate New Era in Earth Observation. *Eos Trans. Am. Geophys. Union* **2014**, *95*, 239–240. https://doi.org/10.1002/2014EO260003.

24. Attema, E.; Snoeij, P.; Davidson, M.; Floury, N.; Levrini, G.; Rommen, B.; Rosich, B. The European GMES Sentinel-1 Radar Mission. In *Proceedings of the IGARSS 2008—2008 IEEE International Geoscience and Remote Sensing Symposium, Boston, MA, USA, 6–11 July 2008*; IEEE: 2008; pp. I–94-I–97; New Jersey; US.
25. Festa, D.; Bonano, M.; Casagli, N.; Confuorto, P.; de Luca, C.; del Soldato, M.; Lanari, R.; Lu, P.; Manunta, M.; Manzo, M.; et al. Nation-Wide Mapping and Classification of Ground Deformation Phenomena through the Spatial Clustering of P-SBAS InSAR Measurements: Italy Case Study. *ISPRS J. Photogramm. Remote Sens.* **2022**, *189*, 1–22. https://doi.org/10.1016/j.isprsjprs.2022.04.022.
26. Psomiadis, E.; Papazachariou, A.; Soulis, K.; Alexiou, D.-S.; Charalampopoulos, I. Landslide Mapping and Susceptibility Assessment Using Geospatial Analysis and Earth Observation Data. *Land* **2020**, *9*, 133. https://doi.org/10.3390/land9050133.
27. Papadopoulos, G.A.; Karastathis, V.; Kontoes, C.; Charalampakis, M.; Fokaefs, A.; Papoutsis, I. Crustal Deformation Associated with East Mediterranean Strike–Slip Earthquakes: The 8 June 2008 Movri (NW Peloponnese), Greece, Earthquake (Mw6.4). *Tectonophysics* **2010**, *492*, 201–212. https://doi.org/10.1016/j.tecto.2010.06.012.
28. Kontoes, C.; Loupasakis, C.; Papoutsis, I.; Alatza, S.; Poyiadji, E.; Ganas, A.; Psychogyiou, C.; Kaskara, M.; Antoniadi, S.; Spanou, N. Landslide Susceptibility Mapping of Central and Western Greece, Combining NGI and WoE Methods, with Remote Sensing and Ground Truth Data. *Land* **2021**, *10*, 402. https://doi.org/10.3390/land10040402.
29. Conforti, M.; Muto, F.; Rago, V.; Critelli, S. Landslide Inventory Map of North-Eastern Calabria (South Italy). *J. Maps* **2014**, *10*, 90–102. https://doi.org/10.1080/17445647.2013.852142.
30. Hooper, A.; Segall, P.; Zebker, H. Persistent Scatterer Interferometric Synthetic Aperture Radar for Crustal Deformation Analysis, with Application to Volcán Alcedo, Galápagos. *J. Geophys. Res.* **2007**, *112*, B07407. https://doi.org/10.1029/2006JB004763.
31. Wang, T.; Zhang, H.; Yang, L.; Dempster, A.G.; Su, C.; Li, K. Landslide Monitoring System Based on Spread-Spectrum Continuous Wave Radar. *In Proceedings of the 2013 IEEE International Geoscience and Remote Sensing Symposium—IGARSS, Melbourne, Australia, 21–26 July 2013*; IEEE: 2013; pp. 4546–4549; New Jersey; US.
32. Alatza, S.; Papoutsis, I.; Paradissis, D.; Kontoes, C.; Papadopoulos, G.A. Multi-Temporal InSAR Analysis for Monitoring Ground Deformation in Amorgos Island, Greece. *Sensors* **2020**, *20*, 338. https://doi.org/10.3390/s20020338.
33. Hu, Z.; Mallorquí, J.J. An Accurate Method to Correct Atmospheric Phase Delay for InSAR with the ERA5 Global Atmospheric Model. *Remote Sens.* **2019**, *11*, 1969. https://doi.org/10.3390/rs11171969.
34. Google (n.d.). [Google Earth Satellite View, Askifou Village]. Available online: https://www.shorturl.at/RTXZ1 (accessed on 27 January 2023).
35. Traffic Interruption Due to rockslides from Machairos to Ramni, Online News of Chania, 20 April 2022, Available online: https://www.haniotika-nea.gr/diakopi-kykloforias-logo-katolisthiseon-vrachon-apo-machairoys-eos-ramni/ (accessed on 12 March 2023).
36. Google (n.d.). [Google satellite view, regional road from Macheri to Ramni]. Available online: https://www.shorturl.at/DJNX2 (accessed on 12 March 2023).
37. Google (n.d.). [Google street view, regional road from Tavronitis to Paleochora, October 2014]. Available online: https://goo.gl/maps/cF76BSPmk4LHKQ9GA (accessed on 12 March 2023).
38. Google (n.d.). [Google street view, regional road from Tavronitis to Paleochora, May 2019]. Available online: https://goo.gl/maps/odC3V1YoBqAWMWQWA (accessed on 12 March 2023).
39. Google (n.d.). [Google Earth Satellite view at Stalos village Jun 2013]. Available online: https://shorturl.at/kwL34 (accessed on 12 March 2023).
40. Google (n.d.). [Google Earth Satellite view at Stalos village May 2022] Available online: https:// shorturl.at/ciBNO (accessed on 12 March 2023).
41. Google (n.d.). [Google street view, motorway outside Stalos village, May 2019]. Available online: https://www.shorturl.at/GHZ17 (accessed on 12 March 2023).
42. Mapillary (n.d.). [Mapillary street view, motorway outside Stalos village, Aug 2022]. Available online: https://rb.gy/ktzz0a (accessed on 12 March 2023).